J. Fluid Mech. (2019), *vol.* 861, *pp.* 585–607.
doi:10.1017/jfm.2018.906

Amplitude modulation between multi-scale turbulent motions in high-Reynolds-number atmospheric surface layers

Hongyou Liu[1], Guohua Wang[1,†] and Xiaojing Zheng[2,†]

[1]College of Civil Engineering and Mechanics, Lanzhou University, Key Laboratory of Mechanics on Disaster and Environment in Western China, Ministry of Education of China, Lanzhou 730000, PR China

[2]Research Center for Applied Mechanics, School of Mechano-Electronic Engineering, Xidian University, Xian 710071, PR China

(Received 17 April 2018; revised 11 September 2018; accepted 6 November 2018; first published online 27 December 2018)

Long-term measurements were performed at the Qingtu Lake Observation Array site to obtain high-Reynolds-number atmospheric surface layer flow data ($Re_\tau \sim O(10^6)$). Based on the selected high-quality data in the near-neutral surface layer, the amplitude modulation between multi-scale turbulent motions is investigated under various Reynolds number conditions. The results show that the amplitude modulation effect may exist in specific motions rather than at all length scales of motion. The most energetic motions with scales larger than the wavelength of the lower wavenumber peak in the energy spectra play a vital role in the amplitude modulation effect; the small scales shorter than the wavelength of the higher wavenumber peak are strongly modulated, whereas the motions with scales ranging between these two peaks neither contribute significantly to the amplitude modulation effect nor are strongly modulated. Based on these results, a method of decomposing the fluctuating velocity is proposed to accurately estimate the degree of amplitude modulation. The corresponding amplitude modulation coefficient is much larger than that estimated by establishing a nominal cutoff wavelength; moreover, it increases log-linearly with the Reynolds number. An empirical model is proposed to parametrize the variation of the amplitude modulation coefficient with the Reynolds number and the wall-normal distance. This study contributes to a better understanding of the interaction between multi-scale turbulent motions and the results may be used to validate and improve existing numerical models of high-Reynolds-number wall turbulence.

Key words: turbulent boundary layers, atmospheric flows

1. Introduction

Turbulent coherent structures that are persistent in time and space are responsible for the production and dissipation of wall-bounded turbulence and thus are important to the understanding of turbulence dynamics (summarized by Robinson 1991; Marusic

† Email addresses for correspondence: ghwang@lzu.edu.cn, xjzheng@xidian.edu.cn

et al. 2010*a*; Dennis 2015). Coherent structures with a large streamwise scale (on the scale of the boundary layer thickness δ and larger), which are commonly termed large-scale motions (LSMs) and very-large-scale motions (VLSMs) or 'superstructures' (Hutchins & Marusic 2007*a*), have been verified to be an important, and perhaps dominant, feature in the outer region of wall turbulence (Tomkins & Adrian 2003; Drobinski *et al.* 2004; Monty *et al.* 2007; Bailey *et al.* 2008; Hutchins *et al.* 2012). The hairpin vortex packet model (Kim & Adrian 1999; Adrian, Meinhart & Tomkins 2000) suggests that LSMs ($\sim 3\delta$) are created by hairpin vortices aligning coherently in the streamwise direction (called the hairpin vortex packet), and packets may also align with other packets to create even larger structures (i.e. VLSMs ($\sim 6\delta$)), where the hairpin vortex is an important elementary coherent structure that explains many features observed in the wall turbulence. LSMs and VLSMs are associated with the wavelengths of the higher and lower wavenumber peaks in the pre-multiplied spectra of the streamwise velocity (Kim & Adrian 1999; Guala, Hommema & Adrian 2006; Balakumar & Adrian 2007; Vallikivi, Ganapathisubramani & Smits 2015), and VLSMs become more dominant in high-Reynolds-number atmospheric surface layer (ASL) flows (Wang & Zheng 2016). These large- and very-large-scale structures carry a substantial portion of the turbulent kinetic energy and Reynolds shear stress (Guala *et al.* 2006; Balakumar & Adrian 2007; Wang & Zheng 2016) and have been found to strongly influence the near-wall cycle through superposition and amplitude modulation (Hutchins & Marusic 2007*b*; Mathis, Hutchins & Marusic 2009*a*; Guala, Metzger & McKeon 2011). The phenomenon of LSM/VLSM amplitude modulation of small-scale motions indicates that the outer region energy may impart to the near-wall region (Mathis *et al.* 2009*a*) and thus contributes to a better understanding of the near-wall turbulence production mechanism (not completely 'autonomous' when referring to the near-wall cycle). Accurately estimating the degree of amplitude modulation is a prerequisite for predictive models of near-wall turbulent motions (Marusic, Mathis & Hutchins 2010*b*; Mathis, Hutchins & Marusic 2011*a*; Mathis *et al.* 2013). Moreover, the phenomenon of amplitude modulation suggests the viability of specifically targeting the large- and very-large-scale structures in order to control turbulence (Hutchins *et al.* 2011; Deng, Huang & Xu 2016). Therefore, studies of amplitude modulation have attracted the attention of many researchers.

The phenomenon of LSMs modulating the amplitude of small-scale energy was originally studied by Brown & Thomas (1977). They performed measurements of the streamwise velocity and the shear stress with an array of hot wires and hot-film wall-shear-stress sensors in a turbulent boundary layer (TBL) at $Re_\tau = 3413$ ($Re_\tau = \delta U_\tau/\nu$ is the friction Reynolds number or Kármán number, where U_τ and ν denote the friction velocity and the kinematic viscosity, respectively). By comparing the low-frequency fluctuations with the rectified high-frequency smoothed signals, they found a high-frequency large amplitude fluctuation occurring near the maximum in the slowly varying part of the signal (in addition to the turbulent duct flow studies of Rajagopalan & Antonia 1980). Based on streamwise velocity time-series data measured in numerous shear flows (including boundary layers, mixing layers, wakes and jets), Bandyopadhyay & Hussain (1984) examined the correlations between the low-frequency signal and a signal similar to the envelope of the high-frequency component. The results indicated a significant coupling between scales in all flows. Using atmospheric data, Hunt & Morrison (2000) found that the large-scale features in the logarithmic layer become dominant and influence the

near-wall region under sufficiently high-Reynolds-number conditions. They categorized the influence as a 'top-down' mechanism that is different from the 'bottom-up' mechanism commonly proposed in lower-Reynolds-number studies. The phenomenon of amplitude modulation was highlighted in Hutchins & Marusic (2007*b*) by studying the fluctuating velocity signals ($Re_\tau = 7300$) acquired in the High Reynolds Number Boundary Layer Wind-Tunnel (HRNBLWT) at the University of Melbourne. They found that the much larger scales in the logarithmic region appear to modulate the amplitude of the small-scale fluctuations as follows: the amplitudes of the small scales were larger within large-scale positive fluctuations, whereas the small scales became relatively quiescent within large-scale negative fluctuations.

The studies mentioned above have demonstrated the presence of the amplitude modulation phenomenon. Based on these observations, Mathis *et al.* (2009*a*) developed a mathematical tool to quantify the degree of the amplitude modulation. They divided the streamwise velocity fluctuations into short- and long-wavelength components by establishing a nominal cutoff wavelength ($\lambda_c = \delta$) and defined the amplitude modulation coefficient (denoted by R_{AM}) by calculating a meaningful correlation coefficient between the long-wavelength components and the filtered envelope of the small-scale fluctuations (obtained via the Hilbert transformation). By comparing the results of single-point and two-point analyses, they suggested that the single-point amplitude modulation coefficient provides a reasonable estimate of the degree of modulation. Moreover, the demodulation procedure was only weakly dependent on the choice of the convection velocity and the cutoff wavelength. Based on this quantitative method, Mathis *et al.* (2009*a*) investigated the amplitude modulation coefficient with laboratory TBL data ($Re_\tau = 2800$–$19\,000$) acquired in the HRNBLWT and ASL data ($Re_\tau = 6.5 \times 10^5$) obtained at the Surface Layer Turbulence and Environmental Science Test (SLTEST) site. They found a high level of correlation near the wall (greater than 0.6), which decreased significantly with the wall-normal distance in the logarithmic region. The amplitude modulation coefficient was found to reach zero at approximately the mid-point of the logarithmic region and become negative at higher wall-normal distances. This indicated a reversal in the modulation behaviour in the upper logarithmic and wake layers; i.e. the small-scale fluctuations were more energetic within large-scale negative fluctuations. They suggested that the negative coefficient may be attributed to intermittency effects at the top of the boundary layer. In addition, they found that the amplitude modulation coefficient increased log-linearly with the Reynolds number in the buffer layer (between the near-wall viscous region and the logarithmic region). Subsequently, Mathis *et al.* (2009*b*) applied the quantitative method to pipe and channel flows ($Re_\tau \approx 3000$) and concluded that the amplitude modulation coefficients (cutoff wavelength $\lambda_c = \delta$) in the internal and external wall-bounded turbulences remain invariant in the inner region, irrespective of the flow case. More recently, studies of the amplitude modulation coefficient have suggested that the wall-normal profile of R_{AM} exhibits a strong resemblance to the skewness profile of the streamwise velocity fluctuations. For example, Schlatter & Örlü (2010) compared the amplitude modulation coefficient ($\lambda_c = \delta$) with the skewness factor using experimental and synthetic streamwise velocity signals ($800 < Re_\tau < 5500$). They found a clearly linear relation between these two physical quantities that have clear fundamental differences and thus concluded that R_{AM} may not be an independent tool for quantifying the degree of amplitude modulation. Mathis *et al.* (2011*b*) further divided the skewness factor into four terms using a scale-decomposed streamwise velocity signal at higher Reynolds number conditions of $Re_\tau = 2800$–$19\,000$. By analysing all of the terms of the

scale-decomposed skewness factor, they suggested that the Reynolds number trend of the skewness factor is strongly related to the amplitude modulation effect and proposed an alternative diagnostic tool for the degree of amplitude modulation.

Based on these studies of the amplitude modulation coefficient, Marusic *et al.* (2010*b*) and Mathis *et al.* (2011*a*) proposed a predictive model with which the statistics of the streamwise velocity fluctuations in the inner region of the wall turbulence can be predicted using only the large-scale velocity information measured in the logarithmic region. Similarly, Marusic, Mathis & Hutchins (2011), Inoue *et al.* (2012) and Mathis *et al.* (2013) presented a fluctuating wall-shear-stress time-series predictive model. These predictive models are significant because the accurate measurements and simulations of the turbulent motion behaviour close to the solid boundary (where the most important physics processes occur) are the most challenging. The effective applications of the amplitude modulation further highlight its importance. Therefore, recent studies on amplitude modulation still attract the attention of many researchers. For example, Talluru *et al.* (2014) extended the amplitude modulation coefficient to all three components of the velocity with measurements from cross-wire probes in the TBL at $Re_\tau = 15\,000$ and found that the modulation of the small-scale energy by the large-scale structures ($\lambda_c = \delta$) is relatively uniform across all three velocity components. Tsuji, Marusic & Johansson (2016) studied the interaction between pressure fluctuations in TBL flows at $Re_\tau = 3585$–6455 and found that the large- and small-scale pressure fluctuations also have a small amplitude modulation effect, but there is a time-lag between them (also observed in previous numerical results for a pipe flow in Luhar, Sharma & McKeon 2014). Squire *et al.* (2016) and Pathikonda & Christensen (2017) explored the inner–outer interactions in rough-wall TBL flows at $Re_\tau = 14\,700$, $z_o^+ = 546$ and $Re_\tau = 4850, 5650$, $z_o^+ = 612, 726$, respectively (as well as the numerical simulations in Nadeem *et al.* 2015; Anderson 2016). By comparing the results with those from the smooth-wall TBL, they found that the rough wall increases the amplitude modulation coefficient ($\lambda_c = \delta$ and $\lambda_c^+ = 7000$), though the roughness effect weakens as the wall-normal distance increases.

In summary, the amplitude modulation of the small scales by LSMs/VLSMs has been widely investigated. However, the vast majority of the studies of amplitude modulation were conducted at low or moderate Reynolds numbers. Because VLSMs become more and more dominant in the wall turbulence with increasing Reynolds number (Hutchins & Marusic 2007*a*,*b*; Wang & Zheng 2016), it is necessary to investigate the VLSM amplitude modulation of the small scales under very-high-Reynolds-number conditions. Previous studies employed a nominal cutoff wavelength (usually taken as δ) to divide the fluctuating velocity into large- and small-scale components. Much less is known about which scales of motion dominate the amplitude modulation and which scales are significantly subject to the modulation effect. This directly affects the accurate estimate of the amplitude modulation coefficient. In addition, studies of the Reynolds number dependence of the amplitude modulation coefficient at high Reynolds numbers are quite scarce. Therefore, the present work aims to investigate the amplitude modulation between multi-scale turbulent motions and its variation with Re_τ based on high-Reynolds-number experimental data obtained from long-term observations in the ASL.

This paper is organized as follows. Section 2 describes the experimental set-up for the field measurements in the ASL at the Qingtu Lake Observation Array (QLOA) site and the data selection and pretreatment. Section 3 introduces the mathematical method used to estimate the degree of amplitude modulation between motions with different length scales. The results for the variation of the amplitude modulation coefficient

with different scales of turbulent motion and the high-Reynolds-number effects of the amplitude modulation coefficient across the logarithmic region are provided in § 4. The conclusions from this study are summarized in § 5.

2. Experimental set-up and data processing

The ASL represents some of the highest Reynolds number conditions that can be achieved terrestrially (Marusic *et al.* 2010*a*); thus, it is seen as a useful benchmark for high-Reynolds-number flow experiments (Guala *et al.* 2011). Therefore, to investigate the amplitude modulation of small scales by LSMs/VLSMs under very-high-Reynolds-number conditions, we performed ASL observations for clean wind (without sand and dust particles) at the QLOA site in western China. The QLOA can perform synchronous multi-point measurements of the three-dimensional turbulent flow field for both wind-blown sand movement and clean wind. This area is passed by a monsoon in the spring, and the soil crust (due to the large salt content) keeps airborne dust to a minimum, which makes it possible to acquire observational data under a large range of wind velocities in the near-neutral ASL. This is beneficial to this study. To date, the ASL observations have been conducted over a duration of more than 7000 h. The three components of the wind velocity and the temperature were measured by sonic anemometers (Gill Instruments R3-50 and Campbell CSAT3B) at a sampling rate of 50 Hz. Twelve sonic anemometer probes were placed on a wall-normal array distributed logarithmically in the vertical direction from $z = 0.5$ to 30 m (where z denotes the wall-normal distance). The fluctuating velocity signals acquired at different heights were employed in the analysis of the amplitude modulation. Additional details about the arrangement of the array, measurement techniques and experimental apparatus can be found in Wang & Zheng (2016).

For these types of ASL observations, the field environmental conditions are complex and uncontrollable. Therefore, to obtain reliable datasets for the analysis of the high-Reynolds-number wall turbulence, it is necessary to perform specific selection and pretreatment on the raw data. The data processing includes correction for the wind direction (Wilczak, Oncley & Stage 2001), steady wind selection (judged by the nonstationary index provided in Foken *et al.* 2004), thermal stability judgment (Monin & Obukhov 1954) and de-trending (Hutchins *et al.* 2012). Following the standard practice in the analysis of ASL data (Wyngaard 1992), the measured data were divided into multiple hourly time series for subsequent analysis to ensure statistical convergence (Hutchins *et al.* 2012). The data processing procedure is consistent with Hutchins *et al.* (2012) and Wang & Zheng (2016) and is not detailed herein. After applying the data processing procedure, 70 sets of high-quality hourly data in the near-neutral ASL are subsequently analysed in this study. The key information relating to the selected datasets is listed in table 1 in appendix A. Wang & Zheng (2016) and Liu, Bo & Liang (2017) performed data validations by checking some basic statistics of these datasets against the existing experimental and theoretical results from canonical zero-pressure-gradient TBL flows. The comparisons confirmed that the selected ASL data acquired at the QLOA site exhibit properties that are typical of canonical TBL flows in general and thus can be used in studies of high-Reynolds-number wall turbulence.

The ASL was approximately neutrally stratified when satisfying the condition of $|z/L| < 0.1$ (Högström 1988; Högström, Hunt & Smedman 2002; Metzger, McKeon & Holmes 2007), where $|z/L|$ is the Monin–Obukhov thermal stability parameter.

In addition, the friction velocity U_τ was estimated by fitting the mean streamwise velocity profile following the chart method of Clauser (1956). The von Kármán constant was adopted as 0.41 according to the ASL studies in Marusic *et al.* (2013). The kinematic viscosity ν was calculated through the barometric pressure and the temperature at the QLOA site (Tracy, Welch & Porter 1980). The ASL thickness δ was estimated based on the streamwise turbulent intensity formula provided in Marusic *et al.* (2013), which is detailed in Wang & Zheng (2016).

3. Estimate of the amplitude modulation coefficient

The single-point amplitude modulation coefficient developed by Mathis *et al.* (2009*a*) is defined as the correlation coefficient between the large-scale component and the filtered envelope of the small-scale fluctuations. It is obtained from the measured streamwise velocity fluctuations as follows. First, the fluctuating streamwise velocity signal u^+ (where $u^+ = u/U_\tau$, and $z^+ = zU_\tau/\nu$ is the inner-flow scaling) is decomposed into large and small components (u_L^+ and u_S^+, respectively). The Hilbert transformation (Spark & Dutton 1972; Sreenivasan 1985; Hristov, Friehe & Miller 1998; Huang, Shen & Long 1999; Ouergli 2002) is then applied on the small-scale fluctuations to extract the corresponding envelope $E(u_S^+)$. The envelope $E(u_S^+)$ represents the changes in the amplitude of these scales, but it tracks not only the large-scale modulation events due to the LSMs/VLSMs in the logarithmic region but also the small-scale variations in the carrier signal. To remove this effect, the envelope is low-pass filtered at the same cutoff wavelength as the large-scale component. Hence, we obtain a filtered envelope $E_L(u_S^+)$ that describes the modulation signal of the small-scale fluctuations by the LSMs/VLSMs. Finally, the meaningful correlation coefficient R_{AM} of the filtered envelope $E_L(u_S^+)$ with the large-scale velocity fluctuation u_L^+ is defined as

$$R_{AM}(z^+) = \frac{\overline{u_L^+ E_L(u_S^+)}}{\sqrt{\overline{u_L^{+2}}}\sqrt{\overline{E_L(u_S^+)^2}}}, \tag{3.1}$$

where $\sqrt{\overline{u_L^{+2}}}$ and $\sqrt{\overline{E_L(u_S^+)^2}}$ denote the root mean squares of the signal u_L^+ and the filtered envelope $E_L(u_S^+)$, respectively. In this study, we employ different cutoff wavelengths, λ_{c1} and λ_{c2}, to obtain the large-scale component u_L^+ ($\lambda_x > \lambda_{c1}$) and the small-scale component u_S^+ ($\lambda_x < \lambda_{c2}$ or $\lambda_{c2} < \lambda_x < \lambda_{c1}$). In addition, these cutoff wavelengths are varied to investigate the amplitude modulation coefficient between multi-scale turbulent motions. That is, the single-point amplitude modulation coefficient from Mathis *et al.* (2009*a*) is used as an indicator, but with varying cutoff wavelengths.

4. Results and discussion

This section explores the amplitude modulation between multi-scale turbulent motions based on the high-Reynolds-number experimental data in the ASL to determine the specific scales of turbulent motions that should be examined when referring to the amplitude modulation. On this basis, the high-Reynolds-number effects of the amplitude modulation in the logarithmic region are examined by plotting R_{AM} at different Reynolds numbers.

4.1. *Amplitude modulation between multi-scale turbulent motions*

According to Guala *et al.* (2006) and Balakumar & Adrian (2007), the motions with length scales between $0.1\pi\delta$ and $\pi\delta$ are termed LSMs, the motions with lengths larger than $\pi\delta$ are VLSMs and the lengths of small-scale motions are shorter than $0.1\pi\delta$, nominally. Therefore, as an example to explore the amplitude modulation between different scales of turbulent motion, the large-scale component is low-pass filtered as $\lambda_x > 3\delta$, and the small-scale components for different cases are filtered as $\lambda_x < 3\delta$, $0.3\delta < \lambda_x < 3\delta$ and $\lambda_x < 0.3\delta$. An example of the resulting decomposition is given in figure 1 for all three cases at the wall-normal location $z \approx 0.006\delta$. Figure 1 shows the decoupling procedure used to calculate the amplitude modulation coefficient, where figure 1(*a*) plots the raw signal u^+ and the very-large-scale component u_L^+ ($\lambda_x > 3\delta$) and figure 1(*b–d*) shows the small-scale fluctuating component u_S^+ ($\lambda_x < 3\delta$ in figure 1I, $0.3\delta < \lambda_x < 3\delta$ in figure 1II and $\lambda_x < 0.3\delta$ in figure 1III), the corresponding envelope $E(u_S^+)$ and the filtered envelope $E_L(u_S^+)$ (black solid line), respectively. In addition, the amplitude modulation of the LSMs ($0.3\delta < \lambda_x < 3\delta$) onto the small scales ($\lambda_x < 0.3\delta$) is shown in figure 1(IV). It should be noted that the motions with scales $0.3\delta < \lambda_x < 3\delta$ are taken as the small-scale component in figure 1(II), whereas they are the large-scale component in figure 1(IV). It is seen in figure 1(I) that an amplitude modulation effect from the VLSMs onto the motions with scales of $\lambda_x < 3\delta$ is visible. The short-wavelength fluctuating signals are more intense during the very-large-scale positive u_L^+ fluctuation (marked with the vertical dashed lines), as observed in the laboratory TBL at low and moderate Reynolds numbers (Hutchins & Marusic 2007*b*; Mathis *et al.* 2009*a*,*b*; Baars, Hutchins & Marusic 2017). The amplitude modulation coefficient is approximately 0.2.

When the fluctuations of $\lambda_x < 3\delta$ are further divided into $0.3\delta < \lambda_x < 3\delta$ and $\lambda_x < 0.3\delta$ components, it is seen in figure 1(II) that the amplitude modulation effect of the VLSMs on the LSMs can be considered to be negligible (as well as the amplitude modulation of LSMs on small scales shown in figure 1IV). The corresponding amplitude modulation coefficients are close to zero. However, figure 1(III) shows that the VLSMs have a more prominent amplitude modulation effect on the small-scale motions of $\lambda_x < 0.3\delta$ than those of $\lambda_x < 3\delta$ in figure 1(I). The amplitude modulation coefficient ($R_{AM} \approx 0.32$) is the maximum of all four cases. In summary, figure 1 suggests a significant difference in the amplitude modulation effect for different scale motions, with the possible indication that the amplitude modulation from the VLSMs is mainly reflected in the small-scale motions, whereas the LSMs are almost unmodulated. This may be due to the fact that both the VLSMs and the LSMs are significantly energetic, though there are differences in the length scales (Guala *et al.* 2006; Balakumar & Adrian 2007; Wang & Zheng 2016).

To investigate in detail the amplitude modulation effect between turbulent motions with different length scales, figure 2 shows R_{AM} for varying large- and small-scale fluctuating components at $z \approx 0.006\delta$. The relatively reliable average results of R_{AM} for datasets with similar Reynolds numbers ($\pm 0.25 \times 10^6$) are presented in figure 2 and the following analyses to reduce the ASL experimental scatter. The corresponding standard deviation is approximately ± 0.11. The results for three Reynolds number intervals ($Re_\tau = (1.9\text{–}2.4)$, $(2.8\text{–}3.3)$ and $(3.4\text{–}3.9) \times 10^6$) are plotted in figure 2 for comparison.

Figure 2(*a*) shows the amplitude modulation effect from the turbulent motions with different large length scales ($\lambda_x > a\delta$, where a varies) onto the small-scale motions ($\lambda_x < 0.3\delta$). It can be seen that R_{AM} increases sharply with a as far as $a = 2.5$ (peak R_{AM}) and then decreases as a continues to increase; i.e. the cutoff

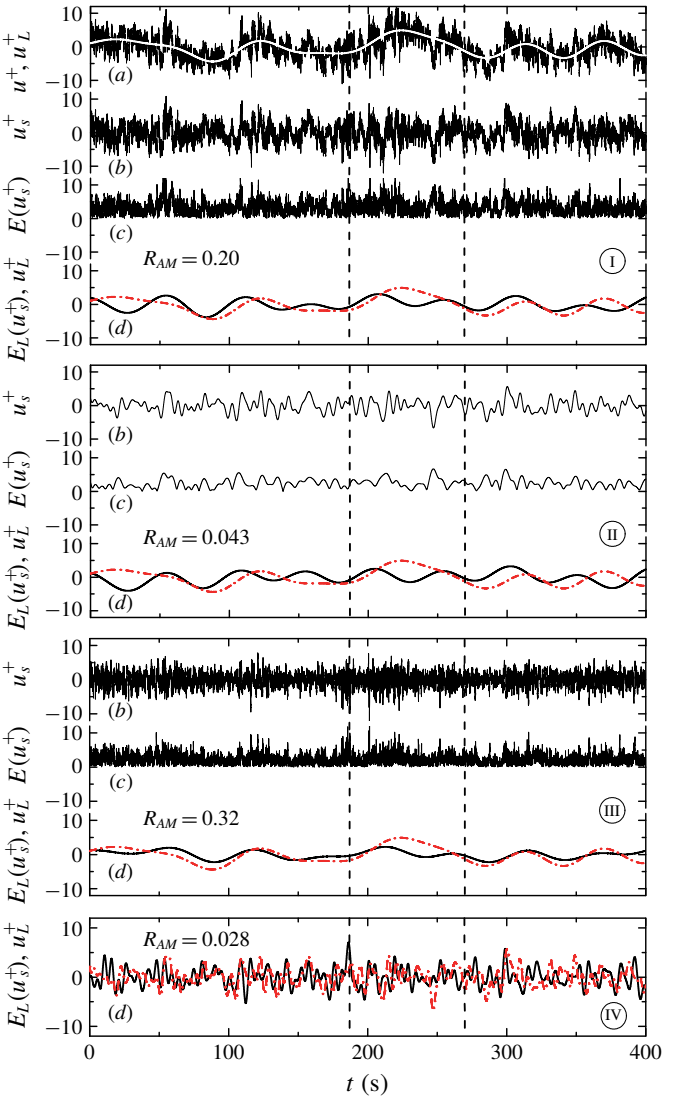

FIGURE 1. (Colour online) Example of scale decomposition of the fluctuating streamwise velocity signal at $z \approx 0.006\delta$ and $Re_\tau \approx 4.6 \times 10^6$ for the amplitude modulation from the VLSMs onto the fluctuating u_S^+ components of (I) $\lambda_x < 3\delta$, (II) $0.3\delta < \lambda_x < 3\delta$ and (III) $\lambda_x < 0.3\delta$. (IV) Amplitude modulation of the LSMs ($0.3\delta < \lambda_x < 3\delta$) onto small scales ($\lambda_x < 0.3\delta$). (*a*) The raw fluctuating signal u^+ and the very-large-scale fluctuation u_L^+ for $\lambda_x > 3\delta$, (*b*) the small-scale component u_S^+, (*c*) the envelope of the small-scale component $E(u_S^+)$ and (*d*) the filtered envelope $E_L(u_S^+)$ (solid line) against the very-large-scale component (red dot-dashed line). For comparison, the mean of the filtered envelope has been adjusted to zero. The dashed vertical lines show regions of positive very-large-scale fluctuations.

wavelength of the large-scale component corresponding to the peak R_{AM} (denoted by λ_{cL-PR}) is approximately 2.5δ. This indicates that the VLSMs with length scales larger than λ_{cL-PR} contribute significantly to the amplitude modulation effect. The VLSM ($\lambda_x > \lambda_{cL-PR}$) amplitude modulation of the turbulence motions with different

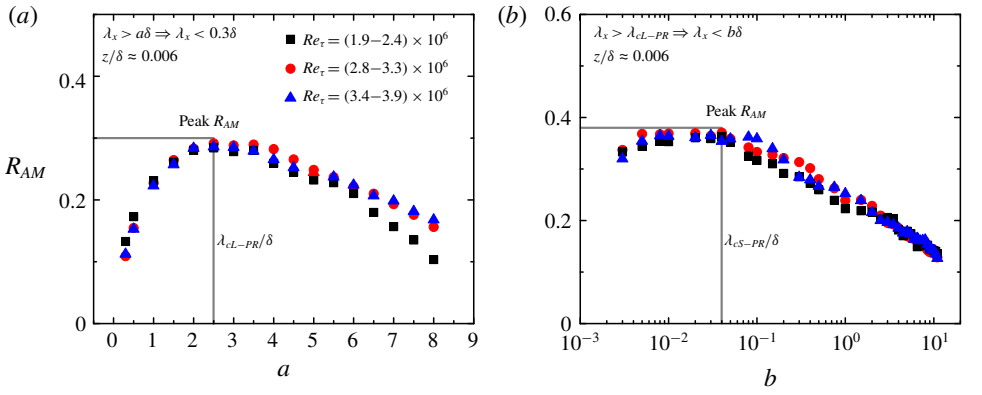

FIGURE 2. (Colour online) Amplitude modulation coefficients between the large- and small-scale components with different length scales at $z \approx 0.006\delta$ for $Re_\tau = (1.9–2.4)$, (2.8–3.3) and (3.4–3.9) $\times 10^6$. (*a*) Amplitude modulation from motions with different large length scales ($\lambda_x > a\delta$, where a varies) onto the small-scale motions ($\lambda_x < 0.3\delta$). (*b*) VLSM ($\lambda_x > \lambda_{cL-PR}$) amplitude modulation of the motions with different short length scales ($\lambda_x < b\delta$, where b varies).

short length scales ($\lambda_x < b\delta$, where b varies) is shown in figure 2(*b*). The abscissa is logarithmic to show the change in R_{AM} more clearly when b is small. Figure 2(*b*) shows that R_{AM} exhibits a gradually slowing increase as $\log(b)$ decreases for all of the Reynolds number conditions, and it appears to level off at approximately $b = 0.04$. Thus, the cutoff wavelength of the small-scale component corresponding to the peak R_{AM} (denoted by λ_{cS-PR}) may be 0.04δ. This suggests that the turbulent motions with length scales shorter than λ_{cS-PR} are more strongly modulated than the other scales of motions. In addition, the variations of R_{AM} with a and b at different Reynolds numbers are qualitatively consistent.

To obtain more information about the amplitude modulation for different scale motions at different heights, the analysis process in figure 2 is repeated for all of the measurement heights in the wall-normal array. As examples, figure 3(*a*,*b*) shows the results for $z \approx 0.003\delta$, 0.006δ, 0.011δ, 0.017δ, 0.033δ, 0.068δ and 0.2δ at $Re_\tau = (2.8–3.3) \times 10^6$. It is seen in figure 3(*a*) that the variations of R_{AM} with a at all of the wall-normal locations are systematic and follow the trend of first increasing and then decreasing. However, there are significant differences in the position of the peak R_{AM}. The cutoff wavelength corresponding to the peak R_{AM} at the lowest measurement height ($z \approx 0.003\delta$) is approximately 1.5δ. With increasing z, λ_{cL-PR} increases, as shown in figure 3(*a*) by the sequence of different symbols. The cutoff wavelength λ_{cL-PR} at the highest measurement height ($z \approx 0.2\delta$) is approximately 10δ. The increase in λ_{cL-PR} indicates that the length scales of the turbulent motions that contribute significantly to the amplitude modulation effect increase with the wall-normal distance. In contrast, the magnitude of the peak R_{AM} decreases with the wall-normal distance. This is expected because the small-scale motions that are subject to the amplitude modulation effect are more significant near the wall. In addition, figure 3(*b*) shows that at all of the heights, R_{AM} appears to level off with decreasing $\log(b)$, and the position at which it levels off (λ_{cS-PR}) also varies with the wall-normal distance. The cutoff wavelength λ_{cS-PR} at $z \approx 0.003\delta$ is approximately 0.02δ, whereas it is approximately 1.5δ at the highest measurement height.

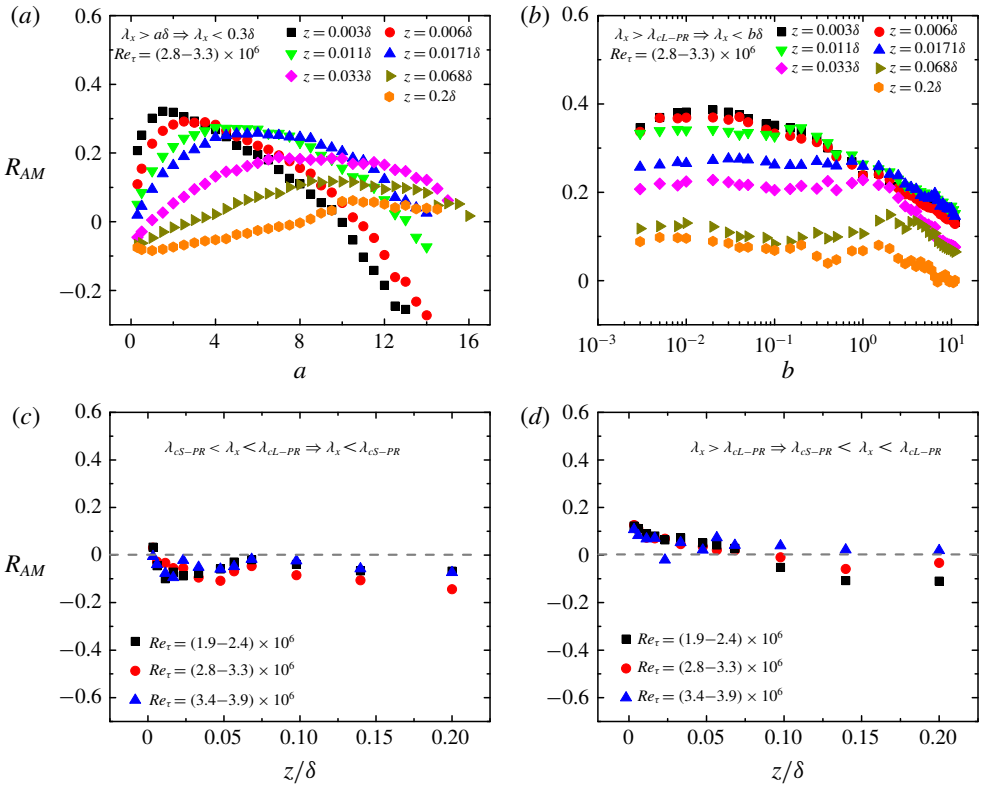

FIGURE 3. (Colour online) Plot of R_{AM} between the large- and small-scale fluctuating components with varying length scales at $z \approx 0.003\delta, 0.006\delta, 0.011\delta, 0.017\delta, 0.033\delta, 0.068\delta$ and 0.2δ for datasets with $Re_\tau = (2.8–3.3) \times 10^6$, where (*a*) and (*b*) are the same as those in figures 2(*a*) and 2(*b*), respectively. (*c*) Plot of R_{AM} from the turbulent motions with scales between λ_{cS-PR} and λ_{cL-PR} onto the small-scale component of $\lambda_x < \lambda_{cS-PR}$ for different Reynolds numbers. (*d*) Amplitude modulation of turbulence motions with scales $\lambda_x > \lambda_{cL-PR}$ on the small-scale component with wavelengths $\lambda_{cS-PR} < \lambda_x < \lambda_{cL-PR}$.

The amplitude modulation related to the turbulent motions with scales between λ_{cS-PR} and λ_{cL-PR} are examined in figure 3(*c*,*d*). Figure 3(*c*) shows the amplitude modulation effect from these motions ($\lambda_{cS-PR} < \lambda_x < \lambda_{cL-PR}$) onto the small-scale component of $\lambda_x < \lambda_{cS-PR}$, and figure 3(*d*) shows the amplitude modulation of the motions with scales larger than λ_{cL-PR} on the small-scale component of $\lambda_{cS-PR} < \lambda_x < \lambda_{cL-PR}$. Within the experimental error, the R_{AM} values in figure 3(*c*,*d*) are found to be close to zero at all heights and Reynolds numbers, though R_{AM} in figure 3(*d*) is slightly larger near the wall. This indicates that the turbulent motions with scales between λ_{cS-PR} and λ_{cL-PR} may have negligible contributions to the amplitude modulation effect, and they are almost unmodulated by the larger motions in the logarithmic region. In summary, figure 3 suggests that at different wall-normal locations, the VLSMs with length scales larger than λ_{cL-PR} contribute significantly to the amplitude modulation effect, whereas other motions with shorter length scales may have negligible contributions; the small-scale motions with wavelengths $\lambda_x < \lambda_{cS-PR}$ are strongly modulated, whereas the larger motions are almost unmodulated. The smaller R_{AM} when $a < \lambda_{cL-PR}/\delta$ (as shown in figure 3*a*) may be due to the confusion

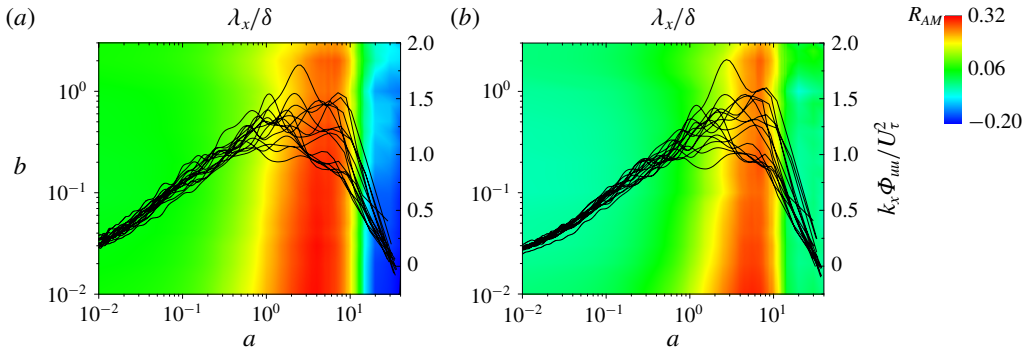

FIGURE 4. Colour contour maps showing the variations of the amplitude modulation coefficient R_{AM} with the length scales of the large-scale components ($\lambda_x > a\delta$) and small-scale components ($\lambda_x < b\delta$) (left vertical axis and bottom abscissa) and the pre-multiplied energy spectra of the streamwise velocity fluctuations $k_x\Phi_{uu}/U_\tau^2$ versus the streamwise wavelength λ_x/δ (right vertical axis and top abscissa): (*a*) $z \approx 0.01\delta$ and (*b*) $z \approx 0.02\delta$. The lines indicate the pre-multiplied energy spectra from 16 sets of hourly data at $Re_\tau = (2.8\text{–}3.3) \times 10^6$.

of the motions that have minor contributions to the amplitude modulation effect in the process of extracting the large-scale modulation signal, and the smaller R_{AM} when $a > \lambda_{cL-PR}/\delta$ may be caused by missing some of the motions that contribute significantly to the amplitude modulation effect. Similarly, the smaller R_{AM} in figure 3(*b*) may also be caused by the confusion of unmodulated signals or by missing some of the signals that are significantly subject to the modulation effect. That is, the inaccurate extraction of the large-scale components (modulating signals) or small-scale components (carrier signals) during the demodulation procedure may result in an underestimation of R_{AM}.

The colour contours of the amplitude modulation coefficient R_{AM} versus the length scales of the large-scale components ($\lambda_x > a\delta$) and small-scale components ($\lambda_x < b\delta$) at $Re_\tau = (2.8\text{–}3.3) \times 10^6$ are shown in figure 4 to gain better insight into the amplitude modulation between the multi-scale turbulent motions. According to Mathis *et al.* (2009*a*), the degree of amplitude modulation is closely related to the energetic signature of the LSMs/VLSMs in the logarithmic region. Therefore, the pre-multiplied energy spectra of the streamwise velocity fluctuations $k_x\Phi_{uu}/U_\tau^2$ (where $k_x = 2\pi/\lambda_x$ denotes the streamwise wavenumber and Φ_{uu} is the power spectral density of the streamwise velocity fluctuations) versus the streamwise wavelength λ_x/δ from the same ASL datasets as the colour contours of R_{AM} are also included in figure 4 for comparison. The analysis of the pre-multiplied spectra follows the methods of Kim & Adrian (1999), Kunkel & Marusic (2006), Vallikivi *et al.* (2015) and Wang & Zheng (2016).

An obvious concentration of the large R_{AM} can be seen in figure 4(*a*,*b*), whereas R_{AM} is close to zero in the other areas. This may mean that not all of the length scales of turbulent motions have an amplitude modulation effect between them; rather, only specific motions do. The large R_{AM} values are concentrated around $a \approx 4$ on the abscissa ($a \approx 5$ in figure 4*b*) and on most of the lower part of the vertical axis (as shown in figure 4*a*,*b* by the red areas). That is, at the outer-scaled wall-normal location of $z \approx 0.01\delta$, the VLSMs with length scales larger than 4δ (5δ for $z \approx 0.02\delta$)

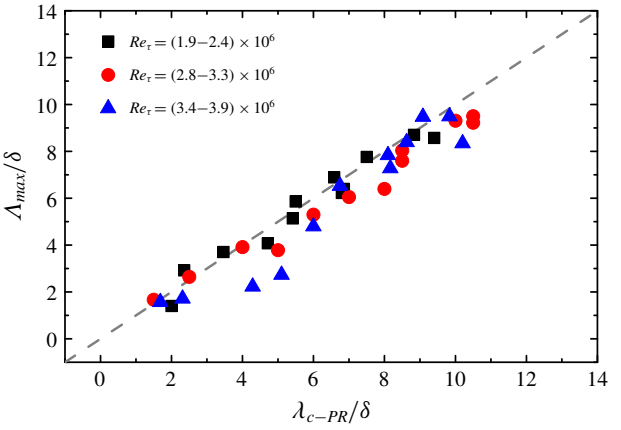

FIGURE 5. (Colour online) Comparison of the large-scale cutoff wavelength corresponding to the maximum R_{AM} (λ_{cL-PR}) and the length scale of the distinct peak corresponding to the VLSMs in the pre-multiplied energy spectra of the streamwise velocity fluctuations (Λ_{max}) for all measurement heights at different Reynolds numbers.

have the most significant contribution to the amplitude modulation effect on the small-scale motions ($\lambda_x < \lambda_{cS-PR}$).

In addition, the pre-multiplied energy spectra of the streamwise velocity fluctuations $k_x\Phi_{uu}/U_\tau^2$ in figure 4 show a distinct peak in the long-wavelength region corresponding to the VLSMs, whereas another peak corresponding to the LSMs is indistinct (as observed in Vallikivi *et al.* 2015; Wang & Zheng 2016). This indicates that the VLSMs in high-Reynolds-number ASL flows may be more dominant than those under lower Reynolds number conditions (Hutchins & Marusic 2007*a*,*b*; Wang & Zheng 2016). A comparison of the pre-multiplied energy spectra with the colour contours of R_{AM} shows that the positions of the distinct peak corresponding to the VLSMs and the concentrated areas of the large R_{AM} are in good agreement. That is, the large-scale cutoff wavelength corresponding to the peak R_{AM} (λ_{cL-PR}) might be consistent with the length scale of the lower wavenumber peak in the pre-multiplied energy spectra of the streamwise velocity fluctuations.

To further investigate the relationship between the large-scale cutoff wavelength corresponding to the peak R_{AM} (λ_{cL-PR}) and the length scale of the lower wavenumber peak in the pre-multiplied energy spectra (denoted by Λ_{max}), figure 5 compares λ_{cL-PR}/δ (abscissa) and Λ_{max}/δ (vertical axis) for all measurement heights at different Reynolds numbers. The low-wavenumber peak was identified as the distinct peak in the long-wavelength region of the energy spectra. At locations where the long-wavelength peak appeared more as a narrow shoulder rather than as a distinct peak, the point of inflection was taken as an estimate of the peak location (following Vallikivi *et al.* 2015). The relatively reliable average results are presented in figure 5, and the corresponding standard deviation is approximately $\pm 2\delta$. The grey dashed line in figure 5 represents the complete consistency of the abscissa and the vertical axis. The current ASL data agree well with the grey dashed line given the experimental scatter; that is, λ_{cL-PR}/δ and Λ_{max}/δ are consistent at all heights and Reynolds numbers. The consistency of λ_{cL-PR} and Λ_{max} means that the most energetic VLSMs with scales larger than the wavelength of the energy spectra peak play a vital role in the amplitude modulation of the small-scale motions. In other words, the existing

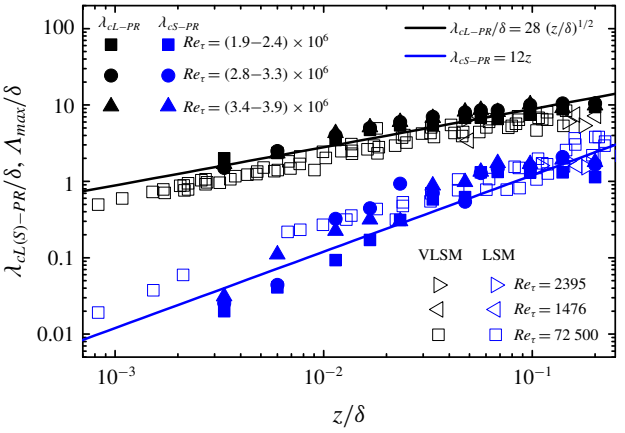

FIGURE 6. Variations of the large- and small-scale cutoff wavelengths (λ_{cL-PR} and λ_{cS-PR}) with the outer-scaled wall-normal distance z/δ. The filled symbols denote the current ASL results for λ_{cL-PR} (filled black symbols) and λ_{cS-PR} (filled blue symbols). The open symbols are the TBL results from Balakumar & Adrian (2007) (Re_τ = 1476, 2395) and Vallikivi *et al.* (2015) ($Re_\tau = 72\,500$) for wavelengths (Λ_{max}) associated with the lower wavenumber peak (VLSMs, open black symbols) and the higher wavenumber peak (LSMs, open blue symbols).

classification of VLSMs, LSMs and small-scale motions is somewhat empirical (Guala *et al.* 2006; Balakumar & Adrian 2007), and the LSMs/VLSMs still contain turbulent motions with various length scales and energetic signatures. The most energetic motions are displayed as the energy peak in the pre-multiplied spectra (Kim & Adrian 1999). In addition, the dominance of energy results in a more prominent effect on the small-scale motions than that on other scales of motions and thus exhibits a peak in the amplitude modulation coefficient.

As shown in figure 3(*a*,*b*), there are significant differences in the large- and small-scale cutoff wavelengths (λ_{cL-PR} and λ_{cS-PR}) at different wall-normal distances. To investigate the dependence of λ_{cL-PR} and λ_{cS-PR} on z, figure 6 plots the changes in λ_{cL-PR} and λ_{cS-PR} versus the outer-scaled wall-normal distance z/δ for all three Reynolds number conditions. The results show that the large-scale cutoff wavelength λ_{cL-PR} increases systematically with z/δ and follows $\lambda_{cL-PR} = 28(z\delta)^{0.5}$, showing simultaneous dependence on the wall-normal distance and the ASL thickness. The small-scale cutoff wavelength λ_{cS-PR} scales with z as $\lambda_{cS-PR} = 12z$. The previously documented TBL data for the wavelengths Λ_{max} associated with the VLSMs (lower wavenumber peak) and the LSMs (higher wavenumber peak) from Balakumar & Adrian (2007) and Vallikivi *et al.* (2015) agree well with the scaling. This scaling is also similar to that for the wavenumbers corresponding to the VLSM peak and the LSM peak (i.e. $k_x\delta \sim (\delta/z)^{0.5}$ and $k_x \sim z^{-1}$, respectively; Vallikivi *et al.* 2015). Therefore, it is appropriate to conclude that in the logarithmic region, the VLSMs with length scales larger than $28(z\delta)^{0.5}$ play a vital role in the amplitude modulation effect, the small-scale motions with scales shorter than $12z$ are significantly subject to the modulation effect and the LSMs with scales ranging between $12z$ and $28(z\delta)^{0.5}$ neither contribute significantly to the amplitude modulation effect nor are strongly modulated.

Therefore, the meaningful correlation coefficient between the VLSMs with scales larger than $28(z\delta)^{0.5}$ and the filtered envelope of the small-scale motions ($\lambda_x < 12z$)

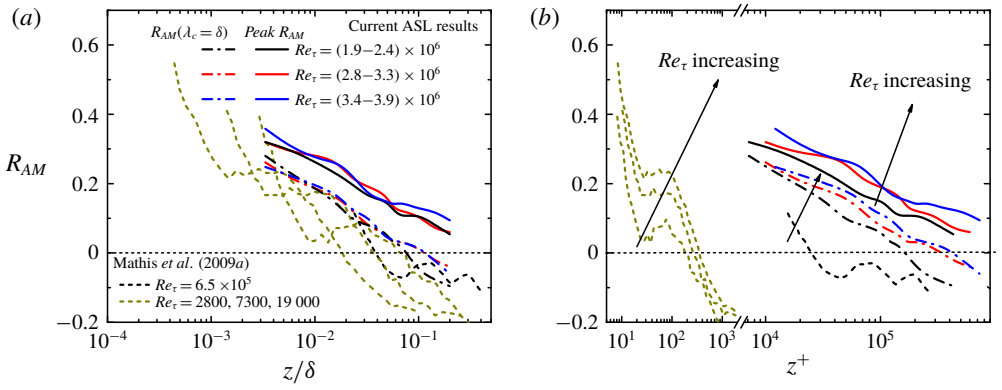

FIGURE 7. Wall-normal profiles of the amplitude modulation coefficient R_{AM} for several Reynolds numbers. The current ASL results are shown by solid and dot-dashed lines, where the solid lines represent the peak R_{AM} and the dot-dashed lines denote R_{AM} $(\lambda_c = \delta)$ estimated by establishing a nominal cutoff wavelength. The laboratory TBL and ASL results available in Mathis *et al.* (2009*a*) are shown by dashed lines. Values of (*a*) R_{AM} plotted in outer-scaled z/δ unit and (*b*) R_{AM} plotted in inner-scaled z^+ unit.

is calculated as an alternative R_{AM} to quantify the amplitude modulation effect more specifically. Following this method, the wall-normal profiles of the calculated R_{AM} (peak R_{AM}, shown by the solid lines) at different Reynolds numbers are shown in figure 7 in terms of the outer and inner scaling and compared with that estimated by establishing a nominal cutoff wavelength, i.e. R_{AM} $(\lambda_c = \delta)$, which is shown by the dot-dashed lines. Figure 7 also includes the results available in Mathis *et al.* (2009*a*) from experiments in a laboratory TBL (HRNBLWT; $Re_\tau = 2800$, 7300 and 19 000) and ASL (SLTEST; $Re_\tau = 6.5 \times 10^5$) flows. In addition to the existence of the amplitude modulation effect in high-Reynolds-number ASLs, figure 7 shows a significant difference between the R_{AM} values obtained by these two methods. The peak R_{AM} is much larger than that estimated by establishing a nominal cutoff wavelength (both for the current ASL results and the previous TBL data, as shown in figure 7*a*) and remains positive in the entire logarithmic region. This is due to the peak R_{AM} specifically targeting the VLSMs that dominate the amplitude modulation and the small-scale motions that are significantly subject to the modulation effect. Moreover, figure 7(*b*) shows that the peak R_{AM} increases with the Reynolds number when inner-scaled with z^+, the details of which will be explored in the next sub-section.

4.2. *High-Reynolds-number effects*

Because few studies have focused on the effects of the Reynolds number on the amplitude modulation under very-high-Reynolds-number conditions, the variation of R_{AM} with Re_τ at different heights in the logarithmic region using all of the selected near-neutral ASL datasets is analysed in this sub-section. As suggested in the previous sub-section, the correlation coefficient between the VLSMs with scales of $\lambda_x > 28(z\delta)^{0.5}$ and the filtered envelope of the small-scale motions $(\lambda_x < 12z)$ can estimate the degree of amplitude modulation more accurately. Therefore, this demodulation procedure is applied to each of the current ASL datasets. The value of R_{AM} $(\lambda_c = \delta)$ calculated by establishing a nominal cutoff wavelength is also analysed as a comparison with the existing results available in the literature. The resulting peak

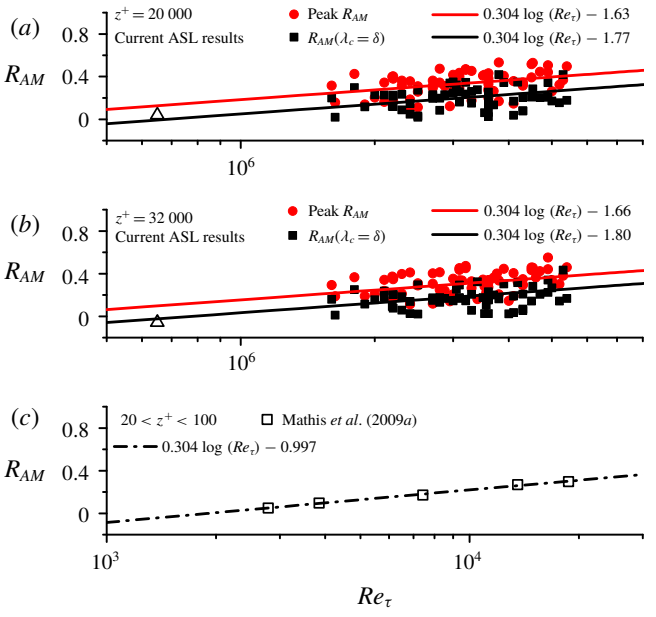

FIGURE 8. (Colour online) Reynolds number evolution of the amplitude modulation coefficient at (*a*) $z^+ = 20\,000$, (*b*) $z^+ = 32\,000$ and (*c*) $20 < z^+ < 100$. The filled symbols denote the current ASL data and the open symbols indicate laboratory TBL and ASL data from Mathis *et al.* (2009*a*). The red circles denote the peak R_{AM} and the black squares are the results calculated by establishing a nominal cutoff wavelength $\lambda_c = \delta$. The lines are the fitting curves.

R_{AM} and R_{AM} $(\lambda_c = \delta)$ are summarized by red circles and black squares, respectively, in figures 8(*a*) and 8(*b*) for $z^+ = 20\,000$ and 32 000. The fixed z^+ is employed in figure 8 to investigate the Reynolds number effects. The previously documented laboratory TBL data for $20 < z^+ < 100$ and the corresponding fitting formula from Mathis *et al.* (2009*a*) are also plotted in figure 8(*c*) for comparison.

The current ASL data in figure 8(*a*,*b*) show that within the experimental scatter, the variations of the peak R_{AM} and R_{AM} $(\lambda_c = \delta)$ with Re_τ at different inner-scaled heights follow an approximately log-linear increase. The previously reported results in the near-neutral ASL acquired at the SLTEST site (shown by the up-pointing triangle) also agree well with the Reynolds number trend of the current ASL data. This trend is consistent with previous work showing that the outer spectral peak and the inner-scaled near-wall peak in the streamwise turbulence intensity both increase log-linearly with the Reynolds number (DeGraaff & Eaton 2000; Metzger & Klewicki 2001; Marusic & Kunkel 2003; Hoyas & Jimnez 2006; Hutchins & Marusic 2007*a*; Hutchins *et al.* 2009; Vallikivi 2014). The outer spectral peak (or 'outer' energy sites) represents the maximum magnitude of the VLSM spectral peak in the outer region (Hutchins & Marusic 2007*a*; Vallikivi *et al.* 2015). This may indicate that the increasing energetic signature of the VLSMs leads to the enhanced amplitude modulation effect on the near-wall cycle, and the increase of the outer energy imparted to the near-wall region (by superposition and modulation) resulting in the near-wall peak of the streamwise turbulence intensity increases with the Reynolds number (Metzger *et al.* 2001; Hutchins & Marusic 2007*a*,*b*). A parametric equation is fitted

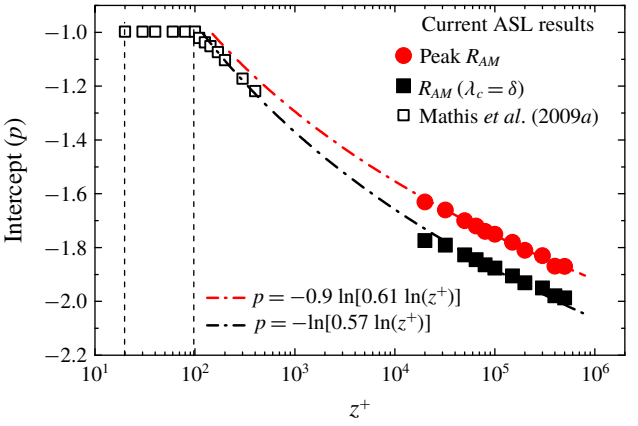

FIGURE 9. (Colour online) Variation of the intercept p with the inner-scaled wall-normal distance z^+. The filled symbols denote the current ASL results and the open symbols are the results obtained by extracting and analysing the laboratory TBL data provided in figure 13(a) of Mathis *et al.* (2009*a*).

to the current ASL data to model the variation of R_{AM} with Re_τ and is given as

$$R_{AM}(z^+) = k \log(Re_\tau) + p, \tag{4.1}$$

which is shown by the solid lines in figure 8(a,b). The log-linear slope k for the current ASL data remains nearly constant (0.28 ± 0.04) at different z^+. To simplify the model parameters, k is taken as 0.304, which is consistent with that for the laboratory TBL data shown in figure 8(c). However, there is a significant difference in the intercept p for varying z^+ due to the decreasing R_{AM} with the wall-normal distance. In addition, the peak R_{AM} is much larger than R_{AM} ($\lambda_c = \delta$) at all Reynolds numbers, which is also reflected in the difference in the intercept p.

To investigate the variation of the intercept p with z^+, the Reynolds number evolutions of the amplitude modulation coefficient are analysed at different values of z^+. The fitted intercept p is plotted in figure 9, where the filled symbols are the current ASL results, and the open symbols are the results obtained by extracting and analysing the laboratory TBL data provided in figure 13(a) of Mathis *et al.* (2009*a*). Figure 9 shows that the intercept p exhibits a gradually slowing decrease with $\log(z^+)$ in the log region, whereas p remains constant in the buffer layer (Mathis *et al.* 2009*a*). The intercept p for the peak R_{AM} is larger than that for R_{AM} ($\lambda_c = \delta$) across the entire logarithmic region. To characterize the variation of p with z^+, parametric equations are fitted to the experimental data and are given as

$$p = -0.9 \ln[0.61 \ln(z^+)], \tag{4.2a}$$

$$p = -\ln[0.57 \ln(z^+)], \tag{4.2b}$$

for the peak R_{AM} (shown by the red dot-dashed line in figure 9) and R_{AM} ($\lambda_c = \delta$) (shown by the black dot-dashed line in figure 9), respectively. Equation (4.2b) agrees well with the current ASL results and also with previously reported laboratory TBL data (Mathis *et al.* 2009*a*).

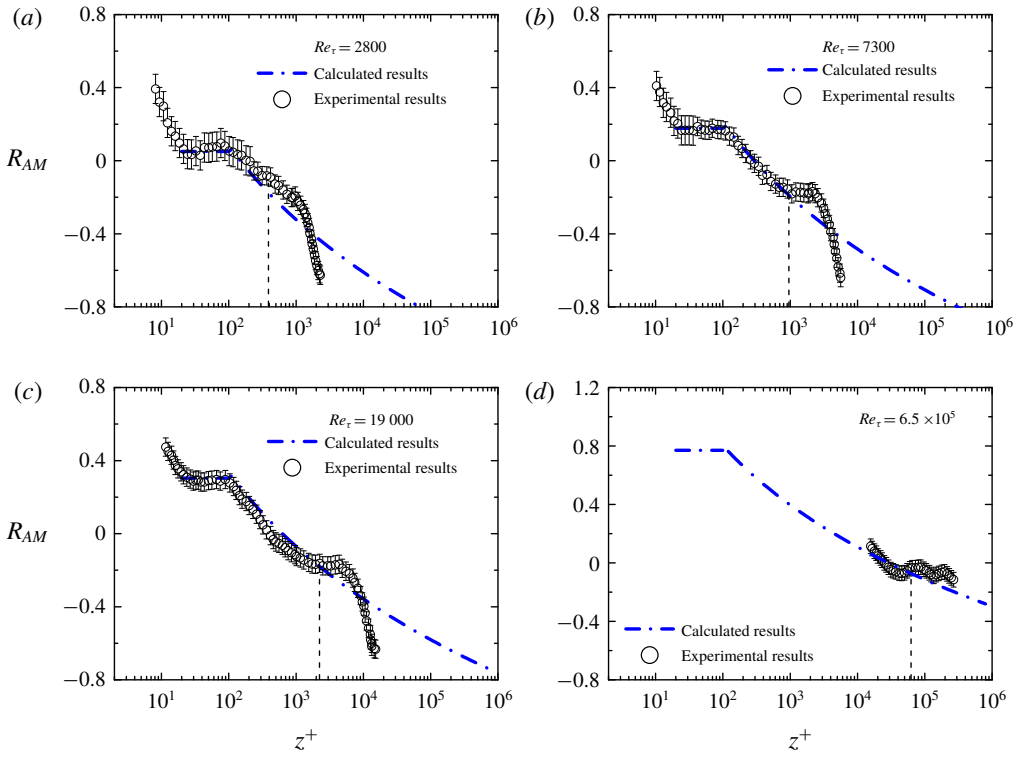

FIGURE 10. (Colour online) Comparison of R_{AM} calculated by the empirical model (dot-dashed line) with the experimental results (open circles) provided in Mathis *et al.* (2009*a*): (*a*) $Re_\tau = 2800$, (*b*) $Re_\tau = 7300$, (*c*) $Re_\tau = 19\,000$, (*d*) $Re_\tau = 6.5 \times 10^5$.

A single model for the amplitude modulation coefficient that accounts for both the Reynolds number and the inner-scaled wall-normal distance can be proposed by replacing the intercept p in (4.1) with (4.2), which is given as

$$R_{AM}(Re_\tau, z^+) = \ln \frac{Re_\tau^{0.132}}{(0.61 \ln z^+)^{0.9}}, \tag{4.3a}$$

$$R_{AM}(Re_\tau, z^+) = \ln \frac{Re_\tau^{0.132}}{0.57 \ln z^+}, \tag{4.3b}$$

for the peak R_{AM} and R_{AM} ($\lambda_c = \delta$), respectively. This empirical model depicts the high-Reynolds-number effects on the amplitude modulation coefficient across the logarithmic region of the boundary layer.

It is prudent to check the results estimated by the proposed empirical model against other experimental results. Most previous studies estimated the amplitude modulation coefficient by establishing a nominal cutoff wavelength. Thus, the results calculated using (4.3*b*) for $z^+ > 100$ (the plateau for $20 < z^+ < 100$ is taken to be the same as the result at $z^+ = 100$) are compared with the laboratory TBL results at $Re_\tau =$ 2800, 7300 and 19 000 and the ASL observational data at $Re_\tau = 6.5 \times 10^5$ (Mathis *et al.* 2009*a*), as shown in figure 10. In figure 10, the dot-dashed line represents the calculated results and the open circles represent the experimental data. The error bars

(± 0.05) indicate the uncertainty in the amplitude modulation coefficient due to the choice of the cutoff wavelength (discussed in Mathis *et al.* 2009*a*). Within the small scatter of the results, the calculated amplitude modulation coefficient agrees well with the laboratory TBL and the ASL results in the logarithmic region (as shown on the left side of the vertical dashed line), spanning over three orders of magnitude in Re_τ. With increasing z^+, the calculated results gradually deviate from the experimental results in the wake region (right side of the vertical dashed line). Therefore, the empirical model of (4.3) provides a plausible estimation of the amplitude modulation coefficient in the logarithmic region ($100 < z^+ < 0.15Re_\tau$) based on the known Reynolds number and the inner-scaled wall-normal distance.

5. Conclusions

Long-term observations in the ASL were performed at the QLOA site, and large amounts of high-Reynolds-number data were obtained. Based on the selected high-quality near-neutral ASL data, the amplitude modulation between multi-scale turbulent motions is investigated under various Reynolds number conditions. A significant difference is found in the amplitude modulation effect for motions with different scales. Further analysis of the amplitude modulation between motions with different length scales indicates that not all of the length scales of turbulent motions have an amplitude modulation effect between them; rather, several specific motions have an effect. The most energetic VLSMs with scales larger than the wavelength of the energy spectral peak in the lower wavenumber region ($\lambda_x > 28(z\delta)^{0.5}$) contribute significantly to the amplitude modulation effect. The small-scale motions with scales shorter than the wavelength of the higher wavenumber peak ($\lambda_x < 12z$) are strongly modulated. However, the motions with scales ranging between $12z$ and $28(z\delta)^{0.5}$ have negligible contributions to the amplitude modulation effect, and they are almost unmodulated.

Therefore, the correlation coefficient between the VLSMs with scales larger than $28(z\delta)^{0.5}$ and the filtered envelope of the small-scale motions ($\lambda_x < 12z$) could provide a more accurate estimate for the degree of amplitude modulation. The corresponding amplitude modulation coefficient (peak R_{AM}) is much larger than that estimated by establishing a nominal cutoff wavelength and remains positive in the entire logarithmic region. Moreover, the peak R_{AM} increases log-linearly with the Reynolds number in the logarithmic region. An empirical model of the amplitude modulation coefficient that accounts for both the Reynolds number and the inner-scaled wall-normal distance is proposed to describe the effects of the Reynolds number across the logarithmic region of the boundary layer. The comparisons of the calculated results with other experimental data at different Reynolds numbers, spanning over three orders of magnitude in Re_τ, confirm that the empirical model provides a plausible estimation for the amplitude modulation coefficient in the logarithmic region ($100 < z^+ < 0.15Re_\tau$).

This work studies the amplitude modulation under very-high-Reynolds-number conditions, which promotes progress in studying the high-Reynolds-number wall-bounded turbulence that is prevalent and important in many engineering and scientific applications. The investigation of the amplitude modulation between motions with different length scales contributes to a better understanding of the interaction between multi-scale turbulent motions. Experimental uncertainties are inevitably associated with these ASL measurements; however, it appears that the ASL measurements can be used as a representation of the very-high-Reynolds-number behaviour.

Acknowledgements

This research was supported by grants from the National Natural Science Foundation of China (nos 11490553, 11232006 and 11702122) and the Fundamental Research Funds for the Central Universities (no. lzujbky-2018-it02). The authors would like to express their sincere appreciation for the support.

Appendix A

No.	Year	Time and date	U_τ (m s^{-1})	Re_τ ($\times 10^6$)	ν ($\times 10^{-5}$ m^2 s^{-1})	z/L	δ (m)
1	2013	13 April 18:00–19:00	0.30	2.4	1.80	0.008	143
2	2013	14 April 08:00–09:00	0.26	2.3	1.72	0.009	152
3	2013	18 April 08:00–09:00	0.35	4.6	1.53	−0.04	201
4	2013	22 April 08:00–09:00	0.27	3.0	1.69	−0.05	185
5	2013	7 May 11:00–12:00	0.26	2.2	1.75	−0.02	148
6	2013	7 May 14:00–15:00	0.34	2.8	1.75	−0.05	143
7	2013	7 May 15:00–16:00	0.36	3.0	1.75	−0.05	146
8	2013	23 May 16:00–17:00	0.34	3.1	1.79	−0.04	163
9	2013	23 May 17:00–18:00	0.36	3.2	1.78	−0.01	158
10	2014	11 April 18:00–19:00	0.29	3.3	1.77	−0.0002	199
11	2014	24 April 08:00–09:00	0.39	3.3	1.60	−0.008	137
12	2014	24 April 09:00–10:00	0.34	2.4	1.59	−0.02	112
13	2014	1 May 06:00–07:00	0.29	2.7	1.63	0.01	151
14	2014	1 May 07:00–08:00	0.28	3.6	1.63	−0.03	208
15	2014	9 May 07:00–08:00	0.20	2.5	1.58	−0.06	194
16	2014	12 May 18:00–19:00	0.26	4.1	1.85	−0.01	289
17	2014	13 May 01:00–02:00	0.35	2.0	1.75	0.03	100
18	2014	14 May 00:00–01:00	0.34	3.2	1.68	0.007	157
19	2014	18 May 19:00–20:00	0.24	2.2	1.77	0.02	159
20	2014	23 May 02:00–03:00	0.26	2.1	1.77	0.03	142
21	2014	23 May 07:00–08:00	0.28	2.2	1.74	−0.04	136
22	2014	23 May 19:00–20:00	0.33	1.9	1.84	0.007	105
23	2014	24 May 04:00–05:00	0.40	4.0	1.74	0.009	174
24	2015	27 March 17:00–18:00	0.33	4.5	1.70	−0.05	229
25	2015	1 April 13:00–14:00	0.42	3.6	1.64	−0.01	140
26	2015	1 April 14:00–15:00	0.42	4.3	1.64	−0.02	166
27	2015	1 April 15:00–16:00	0.44	4.1	1.64	−0.04	152
28	2015	1 April 16:00–17:00	0.37	3.6	1.65	−0.05	160
29	2015	1 April 17:00–18:00	0.28	3.3	1.64	−0.06	193
30	2015	1 April 18:00–19:00	0.27	2.4	1.63	−0.02	145
31	2015	2 April 20:00–21:00	0.30	2.8	1.63	−0.01	152
32	2015	2 April 21:00–22:00	0.27	2.5	1.62	−0.01	150
33	2015	2 April 22:00–23:00	0.29	3.6	1.62	−0.01	201
34	2015	3 April 08:00–09:00	0.19	2.3	1.60	−0.02	190
35	2015	10 April 17:00–18:00	0.40	3.9	1.71	−0.03	165
36	2015	10 April 18:00–19:00	0.34	3.1	1.70	−0.006	155
37	2015	14 April 18:00–19:00	0.31	2.7	1.78	0.01	155
38	2015	15 April 17:00–18:00	0.39	3.7	1.73	−0.04	164

TABLE 1. (continued)

39	2015	15	April	18:00–19:00	0.37	3.5	1.72	−0.007	162
40	2015	30	April	00:00–01:00	0.46	2.1	1.77	0.01	81
41	2015	30	April	04:00–05:00	0.50	5.2	1.71	0.007	177
42	2015	30	April	05:00–06:00	0.51	5.4	1.70	0.005	179
43	2015	30	April	08:00–09:00	0.40	4.3	1.70	−0.02	182
44	2015	7	May	18:00–19:00	0.35	5.3	1.78	−0.03	269
45	2015	9	May	17:00–18:00	0.41	4.9	1.81	−0.04	216
46	2015	9	May	18:00–19:00	0.39	3.6	1.80	−0.004	165
47	2015	10	May	04:00–05:00	0.44	4.7	1.63	0.004	173
48	2015	10	May	07:00–08:00	0.37	3.8	1.64	−0.02	167
49	2015	10	May	08:00–09:00	0.46	4.5	1.65	−0.04	161
50	2015	10	May	18:00–19:00	0.37	5.0	1.68	−0.06	227
51	2015	14	May	18:00–19:00	0.36	4.9	1.79	−0.02	241
52	2015	26	May	22:00–23:00	0.22	1.6	1.79	0.05	130
53	2015	27	May	16:00–17:00	0.34	3.1	1.80	−0.03	163
54	2015	27	May	21:00–22:00	0.41	4.3	1.71	0.002	179
55	2015	29	May	01:00–02:00	0.32	2.5	1.74	0.01	135
56	2015	29	May	02:00–03:00	0.35	1.8	1.73	0.009	89
57	2015	29	May	03:00–04:00	0.35	3.8	1.72	0.007	185
58	2015	29	May	04:00–05:00	0.35	3.6	1.73	0.009	176

TABLE 1. Key information relating to the selected datasets in the neutral ASL.

REFERENCES

ADRIAN, R. J., MEINHART, C. D. & TOMKINS, C. D. 2000 Vortex organization in the outer region of the turbulent boundary layer. *J. Fluid Mech.* **422**, 1–54.

ANDERSON, W. 2016 Amplitude modulation of streamwise velocity fluctuations in the roughness sublayer: evidence from large-eddy simulations. *J. Fluid Mech.* **789**, 567–588.

BAARS, W. J., HUTCHINS, N. & MARUSIC, I. 2017 Reynolds number trend of hierarchies and scale interactions in turbulent boundary layers. *Phil. Trans. R. Soc. Lond.* A **375**, 20160077.

BAILEY, S. C., HULTMARK, M., SMITS, A. J. & SCHULTZ, M. P. 2008 Azimuthal structure of turbulence in high Reynolds number pipe flow. *J. Fluid Mech.* **615**, 121–138.

BALAKUMAR, B. J. & ADRIAN, R. J. 2007 Large-and very-large-scale motions in channel and boundary-layer flows. *Phil. Trans. R. Soc. Lond.* A **365**, 665–681.

BANDYOPADHYAY, P. R. & HUSSAIN, A. K. M. F. 1984 The coupling between scales in shear flows. *Phys. Fluids* **27** (9), 2221–2228.

BROWN, G. L. & THOMAS, A. S. 1977 Large structure in a turbulent boundary layer. *Phys. Fluids* **20** (10), S243–S252.

CLAUSER, F. H. 1956 The turbulent boundary layer. *Adv. Appl. Mech.* **4**, 1–51.

DEGRAAFF, D. B. & EATON, J. K. 2000 Reynolds-number scaling of the flat-plate turbulent boundary layer. *J. Fluid Mech.* **422**, 319–346.

DENG, B. Q., HUANG, W. X. & XU, C. X. 2016 Origin of effectiveness degradation in active drag reduction control of turbulent channel flow at $Re_\tau = 1000$. *J. Turbul.* **17** (8), 758–786.

DENNIS, D. J. 2015 Coherent structures in wall-bounded turbulence. *An. Acad. Bras. Cinc.* **87** (2), 1161–1193.

DROBINSKI, P., CARLOTTI, P., NEWSOM, R. K., BANTA, R. M., FOSTER, R. C. & REDELSPERGER, J. L. 2004 The structure of the near-neutral atmospheric surface layer. *J. Atmos. Sci.* **61** (6), 699–714.

FOKEN, T., GOCKEDE, M., MAUDER, M., MAHRT, L., AMIRO, B. & MUNGER, W. 2004 Post-field data quality control. In *Handbook of Micrometeorology: A Guide for Surface Flux Measurement and Analysis* (ed. X. Lee, W. Massman & B. Law), pp. 181–208. Kluwer Academic.

GUALA, M., HOMMEMA, S. E. & ADRIAN, R. J. 2006 Large-scale and very-large-scale motions in turbulent pipe flow. *J. Fluid Mech.* **554**, 521–542.

GUALA, M., METZGER, M. & MCKEON, B. J. 2011 Interactions within the turbulent boundary layer at high Reynolds number. *J. Fluid Mech.* **666**, 573–604.

HÖGSTRÖM, U. 1988 Non-dimensional wind and temperature profiles in the atmospheric surface layer: a re-evaluation. *Boundary-Layer Meteorol.* **42**, 55–78.

HÖGSTRÖM, U., HUNT, J. C. R. & SMEDMAN, A. S. 2002 Theory and measurements for turbulence spectra and variances in the atmospheric neutral surface layer. *Boundary-Layer Meteorol.* **103** (1), 101–124.

HOYAS, S. & JIMNEZ, J. 2006 Scaling of the velocity fluctuations in turbulent channels up to $Re_\tau = 2003$. *Phys. Fluids* **18** (1), 011702.

HRISTOV, T., FRIEHE, C. & MILLER, S. 1998 Wave-coherent fields in air flow over ocean waves: identification of cooperative behavior buried in turbulence. *Phys. Rev. Lett.* **81** (23), 5245–5248.

HUANG, N. E., SHEN, Z. & LONG, S. R. 1999 A new view of nonlinear water waves: the Hilbert spectrum. *Annu. Rev. Fluid Mech.* **31**, 417–457.

HUNT, J. C. & MORRISON, J. F. 2000 Eddy structure in turbulent boundary layers. *Eur. J. Mech.* B **19** (5), 673–694.

HUTCHINS, N., CHAUHAN, K., MARUSIC, I., MONTY, J. & KLEWICKI, J. 2012 Towards reconciling the large-scale structure of turbulent boundary layers in the atmosphere and laboratory. *Boundary-Layer Meteorol.* **145** (2), 273–306.

HUTCHINS, N. & MARUSIC, I. 2007*a* Evidence of very long meandering features in the logarithmic region of turbulent boundary layers. *J. Fluid Mech.* **579**, 1–28.

HUTCHINS, N. & MARUSIC, I. 2007*b* Large-scale influences in near-wall turbulence. *Phil. Trans. R. Soc. Lond.* A **365**, 647–664.

HUTCHINS, N., MONTY, J. P., GANAPATHISUBRAMANI, B., NG, H. C. H. & MARUSIC, I. 2011 Three-dimensional conditional structure of a high-Reynolds-number turbulent boundary layer. *J. Fluid Mech.* **673**, 255–285.

HUTCHINS, N., NICKELS, T. B., MARUSIC, I. & CHONG, M. S. 2009 Hot-wire spatial resolution issues in wall-bounded turbulence. *J. Fluid Mech.* **635**, 103–136.

INOUE, M., MATHIS, R., MARUSIC, I. & PULLIN, D. I. 2012 Wall shear-stress statistics for the turbulent boundary layer by use of a predictive wall-model with LES. *18th Australasian Fluid Mechanics Conference, Launceston*.

KIM, K. C. & ADRIAN, R. J. 1999 Very large-scale motion in the outer layer. *Phys. Fluids* **11** (2), 417–422.

KUNKEL, G. J. & MARUSIC, I. 2006 Study of the near-wall-turbulent region of the high-Reynolds-number boundary layer using an atmospheric flow. *J. Fluid Mech.* **548**, 375–402.

LIU, H. Y., BO, T. L. & LIANG, Y. R. 2017 The variation of large-scale structure inclination angles in high Reynolds number atmospheric surface layers. *Phys. Fluids* **29** (3), 035104.

LUHAR, M., SHARMA, A. S. & MCKEON, B. J. 2014 On the structure and origin of pressure fluctuations in wall turbulence: predictions based on the resolvent analysis. *J. Fluid Mech.* **751**, 38–70.

MARUSIC, I. & KUNKEL, G. J. 2003 Streamwise turbulence intensity formulation for flat-plate boundary layers. *Phys. Fluids* **15** (8), 2461–2464.

MARUSIC, I., MATHIS, R. & HUTCHINS, N. 2010*b* Predictive model for wall-bounded turbulent flow. *Science* **329** (5988), 193–196.

MARUSIC, I., MATHIS, R. & HUTCHINS, N. 2011 A wall-shear stress predictive model. *J. Phys.: Conf. Ser.* **318**, 012003.

MARUSIC, I., MCKEON, B. J., MONKEWITZ, P. A., NAGIB, H. M., SMITS, A. J. & SREENIVASAN, K. R. 2010*a* Wall-bounded turbulent flows at high Reynolds numbers: recent advances and key issues. *Phys. Fluids* **22** (6), 065103.

MARUSIC, I., MONTY, J. P., HULTMARK, M. & SMITS, A. J. 2013 On the logarithmic region in wall turbulence. *J. Fluid Mech.* **716**, R3.

MATHIS, R., HUTCHINS, N. & MARUSIC, I. 2009*a* Large-scale amplitude modulation of the small-scale structures in turbulent boundary layers. *J. Fluid Mech.* **628**, 311–337.

MATHIS, R., HUTCHINS, N. & MARUSIC, I. 2011*a* A predictive inner–outer model for streamwise turbulence statistics in wall-bounded flows. *J. Fluid Mech.* **681**, 537–566.

MATHIS, R., MARUSIC, I., CHERNYSHENKO, S. I. & HUTCHINS, N. 2013 Estimating wall-shear-stress fluctuations given an outer region input. *J. Fluid Mech.* **715**, 163–180.

MATHIS, R., MARUSIC, I., HUTCHINS, N. & SREENIVASAN, K. R. 2011*b* The relationship between the velocity skewness and the amplitude modulation of the small scale by the large scale in turbulent boundary layers. *Phys. Fluids* **23** (12), 121702.

MATHIS, R., MONTY, J. P., HUTCHINS, N. & MARUSIC, I. 2009*b* Comparison of large-scale amplitude modulation in turbulent boundary layers, pipes, and channel flows. *Phys. Fluids* **21** (11), 111703.

METZGER, M., MCKEON, B. J. & HOLMES, H. 2007 The near-neutral atmospheric surface layer: turbulence and non-stationarity. *Phil. Trans. R. Soc. Lond.* A **365**, 859–876.

METZGER, M. M. & KLEWICKI, J. C. 2001 A comparative study of near-wall turbulence in high and low Reynolds number boundary layers. *Phys. Fluids* **13** (3), 692–701.

METZGER, M. M., KLEWICKI, J. C., BRADSHAW, K. L. & SADR, R. 2001 Scaling the near-wall axial turbulent stress in the zero pressure gradient boundary layer. *Phys. Fluids* **13** (6), 1819–1821.

MONIN, A. S. & OBUKHOV, A. M. F. 1954 Basic laws of turbulent mixing in the surface layer of the atmosphere. *Tr. Akad. Nauk SSSR Geophiz. Inst.* **24** (151), 163–187.

MONTY, J. P., STEWART, J. A., WILLIAMS, R. C. & CHONG, M. S. 2007 Large-scale features in turbulent pipe and channel flows. *J. Fluid Mech.* **589**, 147–156.

NADEEM, M., LEE, J. H., LEE, J. & SUNG, H. J. 2015 Turbulent boundary layers over sparsely-spaced rod-roughened walls. *Intl J. Heat Fluid Flow* **56**, 16–27.

OUERGLI, A. 2002 Hilbert transform from wavelet analysis to extract the envelope of an atmospheric mode: examples. *J. Atmos. Ocean. Technol.* **19** (7), 1082–1086.

PATHIKONDA, G. & CHRISTENSEN, K. T. 2017 Inner–outer interactions in a turbulent boundary layer overlying complex roughness. *Phys. Rev. Fluids* **2** (4), 044603.

RAJAGOPALAN, S. & ANTONIA, R. A. 1980 Interaction between large and small scale motions in a two-dimensional turbulent duct flow. *Phys. Fluids* **23** (6), 1101–1110.

ROBINSON, S. K. 1991 Coherent motions in the turbulent boundary layer. *Annu. Rev. Fluid Mech.* **23**, 601–639.

SCHLATTER, P. & ÖRLÜ, R. 2010 Quantifying the interaction between large and small scales in wall-bounded turbulent flows: a note of caution. *Phys. Fluids* **22** (5), 051704.

SPARK, E. H. & DUTTON, J. A. 1972 Phase angle considerations in the modeling of intermittent turbulence. *J. Atmos. Sci.* **29** (2), 300–303.

SQUIRE, D. T., BAARS, W. J., HUTCHINS, N. & MARUSIC, I. 2016 Inner–outer interactions in rough-wall turbulence. *J. Turbul.* **17** (12), 1159–1178.

SREENIVASAN, K. R. 1985 On the fine-scale intermittency of turbulence. *J. Fluid Mech.* **151**, 81–103.

TALLURU, K. M., BAIDYA, R., HUTCHINS, N. & MARUSIC, I. 2014 Amplitude modulation of all three velocity components in turbulent boundary layers. *J. Fluid Mech.* **746**, R1.

TOMKINS, C. D. & ADRIAN, R. J. 2003 Spanwise structure and scale growth in turbulent boundary layers. *J. Fluid Mech.* **490**, 37–74.

TRACY, C. R., WELCH, W. R. & PORTER, W. P. 1980 Properties of air: a manual for use in biophysical ecology. *Tech. Rep.* 1. Department of Zoology, University of Wisconsin, Madison.

TSUJI, Y., MARUSIC, I. & JOHANSSON, A. V. 2016 Amplitude modulation of pressure in turbulent boundary layer. *Intl J. Heat Fluid Flow* **61**, 2–11.

VALLIKIVI, M. 2014 Wall-bounded turbulence at high Reynolds numbers. PhD thesis, Princeton University.

VALLIKIVI, M., GANAPATHISUBRAMANI, B. & SMITS, A. J. 2015 Spectral scaling in boundary layers and pipes at very high Reynolds numbers. *J. Fluid Mech.* **771**, 303–326.

WANG, G. H. & ZHENG, X. J. 2016 Very large scale motions in the atmospheric surface layer: a field investigation. *J. Fluid Mech.* **802**, 464–489.

WILCZAK, J. M., ONCLEY, S. P. & STAGE, S. A. 2001 Sonic anemometer tilt correction algorithms. *Boundary-Layer Meteorol.* **99**, 127–150.

WYNGAARD, J. C. 1992 Atmospheric turbulence. *Annu. Rev. Fluid Mech.* **24**, 205–233.